DETERMINING BCP ETCH RATE AND UNIFORMITY IN HIGH LUMINOSITY LHC CRAB CAVITIES

T. Jones[1], S. Pattalwar, STFC Daresbury Laboratory, Warrington, UK
G. Burt, J. Mitchell, University of Lancaster, Lancaster, UK
L. Marques Antunes Ferreira, R. Calaga, O. Capatina, R. Leuxe, CERN, Geneva, Switzerland
S. Verdu-Andres, B.Xiao, Brookhaven National Laboratory, Upton, USA
[1]also at University of Lancaster, Lancaster, UK

Abstract

The compact SRF Crab Cavities required for HL-LHC have complex geometries making prediction of average and local BCP etch rates a difficult task. This paper describes a series of experiments and simulations used to determine the etch uniformity and rate within these structures. An initial experiment was conducted to determine the correlation between etch rate and flow rate in a simple Nb tube. These results were then incorporated into Computational Fluid Dynamics simulations of acid flow in the Double Quarter Wave (DQW) cavity to predict etch rates across the surface and allow optimisation of the BCP setup. There were several important findings from the work; one of which is that the flow rate in the relatively large body of the cavity is predominantly driven by natural convection due to the exothermic reaction. During BCP processing of the DQW cavity a significant difference in etching was observed between upper and lower horizontal surfaces which was mitigated by etching in several orientations. Two DQW cavities manufactured by CERN have received a heavy BCP of 200 µm followed by 2 light BCPs of 20 µm each. Subsequent testing has shown performance exceeding required accelerating gradient and Q factor.

INTRODUCTION

There are several previous studies investigating the fluid flow of Buffered Chemical Polishing (BCP) acid within elliptical cavities [1, 2, 3]. In these studies it is common that a baffle be designed in order to give uniform flow speed within the cavities. Without baffles the etch rate at the iris of an elliptical cavity is typically twice that of the equator [4]. Another technique which has been proven to give good cavity performance is rotation of the cavity. This paper shows that this is most likely due to providing agitation of the acid in all areas of the cavity rather than providing uniform flow rate. For the complex shape of the Double Quarter Wave (DQW) SRF Crab Cavity (Fig. 1) the design of baffles to steer flow would be a time consuming process, and rotating the cavity would also require a significant hardware investment within the CERN BCP facility. It was therefore decided that the DQW prototype cavity would be etched in fixed positions, with varying orientations and flow ports to give an approximately uniform flow. Computational Fluid Dynamics (CFD) was used to identify the orientations with the most uniform (lowest standard deviation) flow condition. An experiment was performed to derive a correlation between etch rate and acid flow rate. This was used to predict the material removal rates at the surfaces of the cavity and to provide the average removal rate. The cavity was then etched and non-uniformities in etching were observed due to the low flow in the cavity.

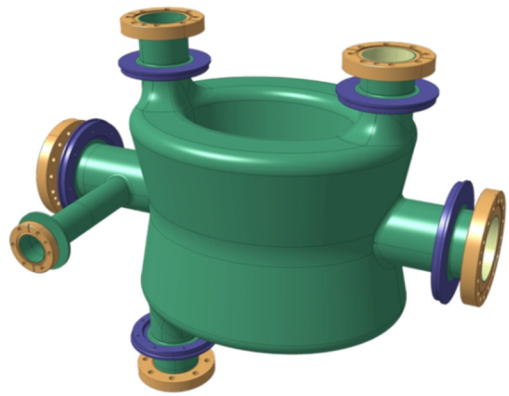

Figure 1: Double Quarter Wave SRF Crab Cavity.

DQW BCP CFD SIMULATION

CFD analysis was performed using ANSYS CFX [5] to identify the flow speed of acid throughout the volume of the DQW cavity in 8 different orientations, Fig. 2. Range (maximum minus minimum), standard deviation and mean average flow speed were evaluated across 21 monitor points distributed within the cavity volume. The boundary conditions for the analyses were as follows:

- The dynamic viscosity of acid used was 0.022 Ns/m^2 [1].
- A total flow of 6 litres per minute was distributed equally across the 3 inlets.
- The density of the acid used was 1458 kg/m^3.
- Buoyancy was turned on, with 9.81 m/s^2 applied in the direction shown in Fig. 2.
- Acid specific heat capacity 2090 J/kg/K [6].
- Tests were performed in each orientation with and without 1200 W/m^2 applied to all cavity surfaces to represent heat from the exothermic reaction [7].
- Results were obtained for a rotating cavity at 0.7 rev/min, one 50% (50) and one 90% full of acid (90), with 6 L/min flow through one beam port. For this a rotating mesh was used in a transient multi-phase analysis lasting 90 seconds (Fig. 3).

ISBN 978-3-95450-191-5

Simulation Results and Comparison

Simulation results are summarised in Table 1. Subscript 'a' indicates a study case for which no exothermic reaction was considered; subscript 'b' refers to a study case for which the estimated 1200 W/m^2 heat was applied to all surfaces. In the majority of cases the average flow speed is higher with the heat of reaction included. The flow speeds are so low that the natural convection due to this heat is driving the flow within the cavity. The results for a rotating cavity show larger flow deviations (i.e. less uniformity) but significantly higher flow speeds and therefore agitation of the acid, which is deemed to be advantageous. From the two rotating scenarios, a higher average fluid velocity is observed in the cavity that was 90% full of acid. The rotation speed was the same for both cavities, but the total mass differs due to the different acid volume. Thus the 90% full cavity shows a greater kinetic energy, which results in a more turbulent flow leading to higher local velocities with a broader range.

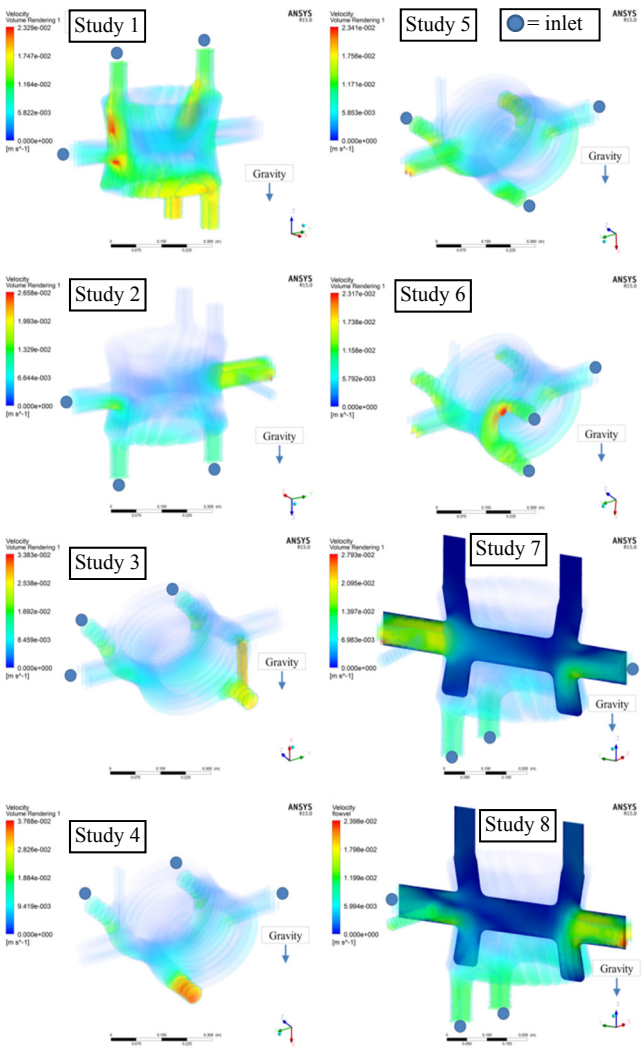

Figure 2: Cavity orientations and acid flow speed plots from ANSYS CFX with heat of reaction turned on.

Table 1: Results of Flow Speed Simulations in 8 Orientations With and Without Heat of Reaction.

Study No.	Range (mm/s)	Standard deviation (mm/s)	Average velocity (mm/s)
1_a	6.24	1.63	1.93
1_b	12.67	3.51	6.04
2_a	22.14	4.67	3.16
2_b	20.14	4.40	2.93
3_a	10.99	2.56	2.60
3_b	6.73	2.00	3.04
4_a	6.25	1.75	2.19
4_b	6.51	1.76	2.66
5_a	13.76	3.21	1.97
5_b	11.67	2.59	4.14
6_a	10.57	2.51	1.68
6_b	14.76	3.59	4.03
7_b	21.95	4.57	3.92
8_b	16.86	4.06	2.87
$Rotating_{50}$	17.34	5.78	6.94
$Rotating_{90}$	49.92	6.97	15.65

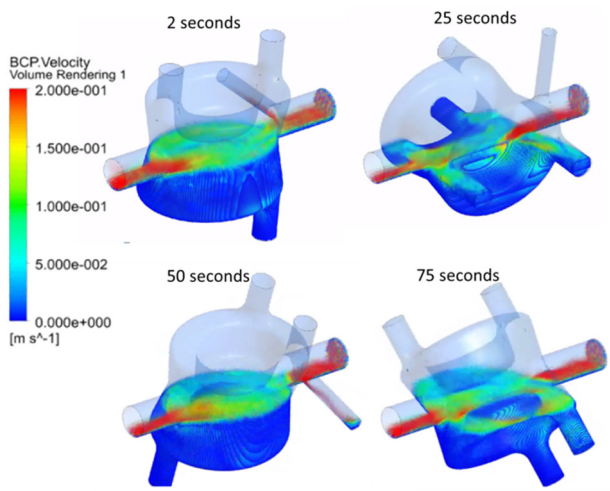

Figure 3: Flow speed analysis of rotating cavity.

FLOW SPEED TO ETCH RATE CORRELATION EXPERIMENT

An experiment was designed to determine a correlation between acid flow rate and etch rate, which could then be combined with the simulated results to estimate etching rates within the cavity. Custom seals were designed to fit an ID 35.7 mm Niobium tube into a sealed BCP system. A variable speed diaphragm pump was used to vary the flow speed through the tube from 80 mm/s to 150 mm/s to 220 mm/s. The mass of the tube was measured accurately before and after being exposed to the acid to calculate material removal. The samples were exposed to

ISBN 978-3-95450-191-5

the acid for an average of 30 minutes in order to obtain significant etching and therefore a higher ratio of material removal to measurement error. An Olympus 38DLP ultrasonic head was also used to validate the change in tube thickness. Separately a flat plate sample was suspended vertically in the acid bath to determine the etch rate with a natural convection condition. The temperature of the bath was stabilised using heat exchange with large capacity chiller. The experiments were performed at 3 temperatures: 6.5°C, 11°C and 15°C. Due to the high volume of the acid bath it was determined that acid saturation would not affect the results. The experimental setup is shown in Fig. 4.

Experiment Results

The results show a strong relationship between the flow speed of acid and the etch rate at the Nb surface, Fig. 5. Due to the non-linearity of this correlation the etch rate is more critical at low flow speeds. From a natural convection condition to flow at 80 mm/s there is approximately a factor of 2 increase in etching rate. The relationship between bulk acid temperature and etch rate appears to be linear, Fig. 6.

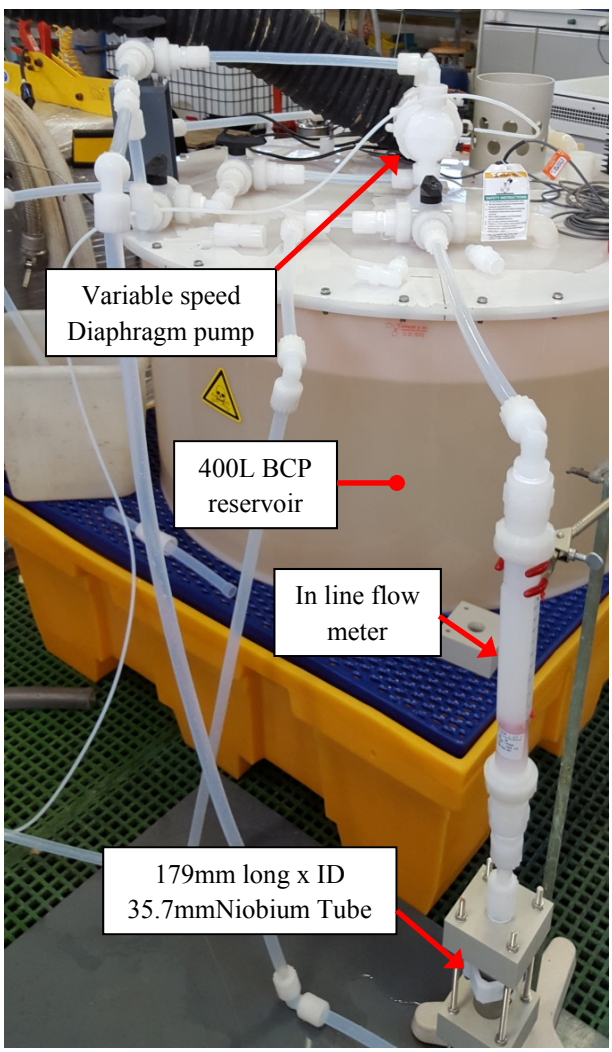

Figure 4: Flow rate to Etch Rate experimental setup.

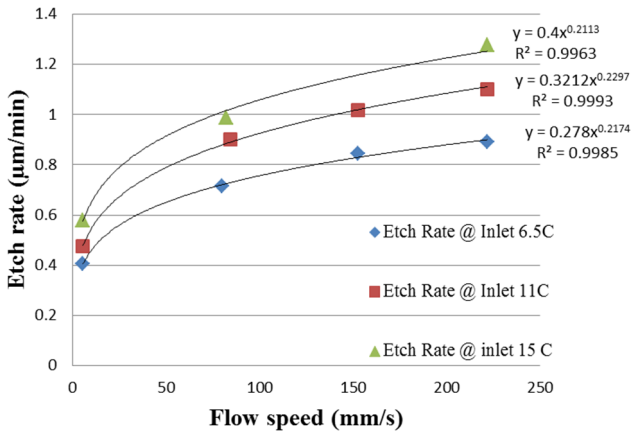

Figure 5: Etch rate to flow speed results.

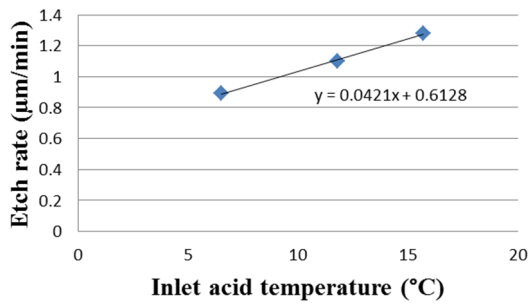

Figure 6: Etch rate variance against bulk acid temperature at fixed flow speed of 220 mm/s.

Combining Experimental Results With CFD Simulations

The velocity of a fluid at a surface is zero [8], however, one can calculate the turbulence kinetic energy (TKE) at the surface. Therefore to determine etch rate at a surface within a CFD simulation, a TKE to etch rate relationship was required. A CFD model of the Nb tube used in the experiment was created and this model was then utilised to identify the TKE at the surface of the tube for each of the flow rates tested, this was then combined with the etching rate data to generate the following relationship (at 11°C):

$$\text{Etch Rate} = 3.1585 \times \text{TKE}^{0.183}$$

This relationship was written into ANSYS CFX as a custom function and etch rate was plotted as a variable in CFX-Post, Figure 7. The average etching rate in the cavity was found to be 0.46 µm/min at 11°C, equivalent to the etching rate of the sample suspended in the BCP bath i.e. a natural convection flow condition. The etching rate across the cavity body was fairly uniform, ranging from 0.40 µm/min to 0.49 µm/min. In all cavity orientations the highest etching rates were observed at the beam ports and beam port blending, in which etching rates up to 0.60 µm/min could be observed. RF frequency sensitivity is shown to be comparatively low in these regions.

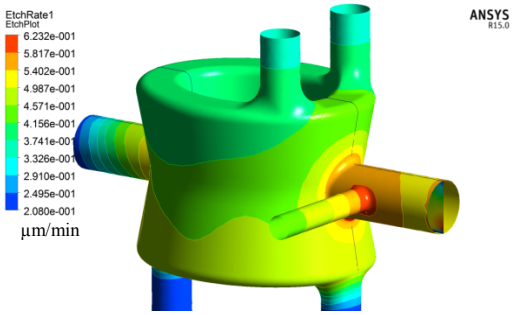

Figure 7: Etch rate plot from ANSYS CFX.

ESTIMATED RF FREQUENCY SHIFTS

The total RF frequency shift resulting from BCP was evaluated initially by comparing the frequency of the nominal cavity (after BCP, with 4 mm-thick walls) with the frequency of the same cavity with uniformly thicker walls (pre-BCP). Cavity models for each scenario were prepared in CATiA [9]. The frequency of each model was computed using CST Microwave Studio [10]. A uniform removal of 210 µm gave a decrease of 170 kHz in cavity RF frequency. The volume variations expected from BCP (in the order of tenths to hundreds of µm) are small perturbations of the cavity volume. Thus, the Slater's theorem [12] was used to estimate the frequency sensitivity associated to a local volume variation due to BCP.

The Slater's Theorem

The frequency shift $\Delta\omega$ associated to a small perturbation of the resonant cavity volume dV can be calculated using the Slater's theorem:

$$\frac{\Delta\omega}{\omega_0} \approx \frac{\Delta W_m - \Delta W_e}{W_m + W_e} = \frac{\int_{\Delta V}(\mu|H_0|^2 - \varepsilon|E_0|^2)dV}{\int_{V_0}(\mu|H_0|^2 + \varepsilon|E_0|^2)dV},$$

where ω_0 is the resonant frequency of the unperturbed cavity, W_m and W_e are the magnetic and electric stored energies in the unperturbed cavity, ΔW_m and ΔW_e are the variations in magnetic and electric stored energy, μ is the magnetic permeability of the cavity interior, ε is the electric permittivity and, H_0 and E_0 are the magnetic and electric field distributions, respectively, in the unperturbed cavity with volume V_0. The cavity frequency increases if the shape is pushed inwards in a region with high magnetic field and the frequency decreases if this occurs in a region with high electric field.

Local Frequency Sensitivities in a DQW

Electric and magnetic field values for the operating mode of the DQW cavity were extracted from a simulation conducted with the eigenmode solver of CST Microwave Studio. Electric and magnetic energy density distributions for the DQW cavity are shown in Figure 8. The highest electric field region is found between the so-called 'capacitive plates' of the DQW cavity. The highest magnetic field region is located in the so-called 'cavity dome'. These regions show the largest frequency sensitivity to volume variation. The frequency sensitivities listed in Table 2 result from increasing the cavity volume locally by a small amount, Δt (comparable to removing material from the inner cavity surface).

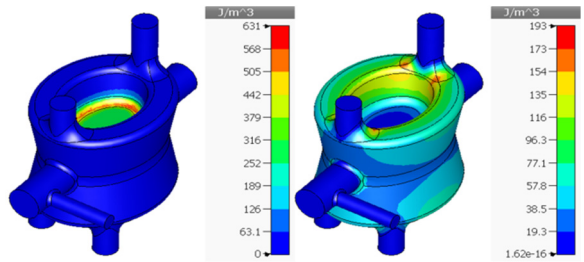

Electric energy density Magnetic energy density

Figure 8: Distributions of electric and magnetic energy density for fundamental mode of the DQW cavity.

Table 2: Frequency Sensitivity Δf/Δt for the Different Cavity Regions Shown in Fig. 9.

Region	Label	$\Delta f/\Delta t$ (kHz/µm)
Capacitive plates	A	+4.24
Inductive plates	B	-1.74
Outer conductor wall	C	-3.06
Inner conductor wall	D	-2.26
Two beam port tubes	E	-0.14
Four small port interfaces	F	-1.19
Four small port tubes	G	-0.02
Blend capacitive plate edges	H	+4.62
Blend inner wall edges	I	-1.22
Blend outer wall edges	J	-1.10
Blend cavity waist	K	-0.32
Blend outer wall edges	L	-1.10

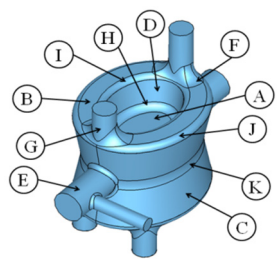

Figure 9: Assignment of labels used in Table 1 to different regions of the DQW cavity.

BCP PROCESSING OF DQW CAVITY

The two SPS DQW Crab cavities were BCP processed at CERN between January and April 2017. The cavities were each processed in the 4 orientations/configurations shown in chronological order in Figure 10. A hydrogen degassing thermal treatment was performed on each cavity between heavy and light BCP.

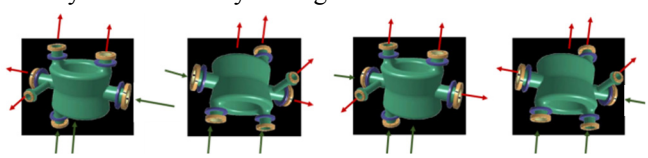

Figure 10: BCP process steps (From left to right).

ISBN 978-3-95450-191-5

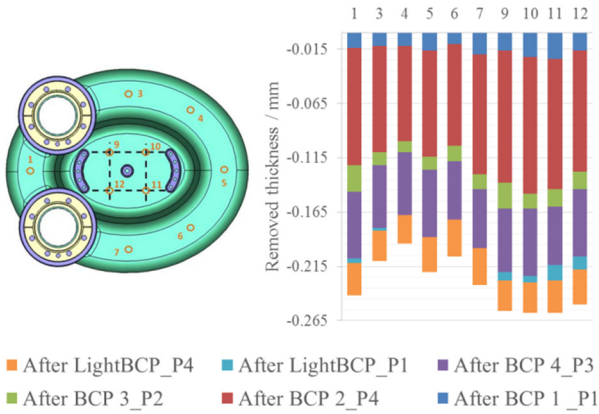

Figure 11: Material removal from lower part of cavity.

The overall results for the chemical polishing/etching rate were comparable with previous data obtained from the proof-of-principle cavity [11] and from CFD simulations. As expected, the pump flow rate of 11 L/min provides fluid dynamics conditions inside the cavity very close to purely natural convection regime. The average etching rate varied between 0.4 to 0.53 µm/min across all processing steps and both cavities. Once the steady state regime was established, in less than 10 minutes, the average temperature ranged from 10.2 to 13.7°C, with a maximum ΔT across inlet and outlet of about 2°C,. The average etching rate was calculated using the surface area and weight difference of the cavity, before and after each BCP step. The bath temperature was measured in the storage tank close to the circulating pump feed pipe and at the return pipe.

While the average results were coherent with previous work, local etching rates in each individual process step presented fairly significant variations to the CFD predictions. Figure 11 shows material removal at various locations on the base of the cavity. Wall thickness measurements were made using a SN60 Krautkramer n° 00PTD9 with a flat transductor ALPHA-2 n° 024J52 de 15MHz. Local etching rates vary significantly depending on the cavity orientation. Surfaces facing upwards are etched significantly less than surfaces facing downwards. This behaviour was observed on the surfaces of both cavities. Acid pumping speed and temperature were constant throughout each step and for each cavity, thus gravity was deemed to be responsible for the observed dependence of the local etching rate on the surface orientation. We suspect that, as result of low flow rates, heavier neutral products of the reaction will rest on the surfaces facing upwards, preventing them from being etched. Etching the cavities in two different orientations mostly averaged this effect out.

The inner capacitive plates were etched approximately 40µm more than the outer conductive plates. Considering the local frequency sensitivities in Table 2, the different etching between capacitive and inductive plates (respectively, regions A and H) might explain why the cavity frequency increased by 140 kHz after BCP instead of decreasing by 170 kHz as it was predicted.

CONCLUSION

Computational Fluid Dynamics was used to predict acid flow within the HL-LHC DQW Crab Cavity. Combined with experimental results this data was used to predict etching rates at the internal surfaces of the cavity. While the average etching rate matched the real processing results of the cavity, the localised results varied. A gravitational effect was discovered in that lower horizontal surfaces are etched significantly less than upper horizontal surfaces. BCP in a rotating bench may provide more uniform etching in complex geometry cavities such as the DQW. This rotation would provide more agitation of the acid, thus limit gravitational and stagnation effects. Plans are in place at CERN to develop a rotating bench for BCP of SRF cavities.

REFERENCES

[1] C. Boffo, "Optimization of the BCP processing of elliptical NB SRF cavities," in *Proc. EPAC 2006*, Edinburgh, Scotland, June 2006, paper MOPCH174, pp 469-471.

[2] M. Trabia, "Optimization Of Chemical Etching Process In Niobium Cavities," in *Proceedings of American Society of Mechanical Engineers International Design Engineering Technical Conference*, Salt Lake City, 2004.

[3] I. Malloch, "SRF cavity processing and chemical etching development for the FRIB LINAC", in *Proc. SRF2015*, Whistler, BC, Canada, Sept 2015, paper MOPB095, pp. 373-377.

[4] P. Michelato, "SC Cavity Fabrication Technology and Industrialization," 1-2 October 2013. [Online]. http://ipnwww.in2p3.fr/MAX/images/stories/freedownloads/MAXschool_Michelato.pdf. *[Accessed 27 June 2017].*

[5] ANSYS, *ANSYS CFX,* 2015.

[6] C. Preston, https://people.nscl.msu.edu/~hartung/phptry/srf/pdf/Etch_Test.pdf, 21 June 2000. [Online].

[7] C. Cooper, "Optimization of the BCP processing of elliptical Nb SRF cavities", in *Proc. SRF2007*, Beijing, China, Oct 2007, paper TUP70, pp. 308-312.

[8] J. F. Douglas, Fluid Mechanics, Prentice Hall; 4 edition , 2000.

[9] Dassault, *CATIA,* V5.32.

[10] CST AG, *Computer Simulation Technology Program,* Darmstadt, 2016.

[11] S. Verdú-Andrés, "Prototyping experience for the LHC DQW crab cavities," in *TTC 2017 Meeting*, Lansing, 2017.

[12] J. C. Slater, "Microwave Electronics," *Reviews of Modern Physics,* vol. 18, no. 4, pp. 441-512, 1946.